Cell Stem Cell
Article

Specific MicroRNAs Are Preferentially Expressed by Skin Stem Cells To Balance Self-Renewal and Early Lineage Commitment

Liang Zhang,[1] Nicole Stokes,[1] Lisa Polak,[1] and Elaine Fuchs[1,*]
[1]Howard Hughes Medical Institute and Laboratory of Mammalian Cell Biology and Development, The Rockefeller University, New York, NY 10065, USA
*Correspondence: fuchslb@rockefeller.edu
DOI 10.1016/j.stem.2011.01.014

SUMMARY

Increasing evidence suggests that microRNAs may play important roles in regulating self-renewal and differentiation in mammalian stem cells (SCs). Here, we explore this issue in skin. We first characterize microRNA expression profiles of skin SCs versus their committed proliferative progenies and identify a microRNA subset associating with "stemness." Of these, miR-125b is dramatically downregulated in early SC progeny. We engineer an inducible mice system and show that when miR-125b is sustained in SC progenies, tissue balance is reversibly skewed toward stemness at the expense of epidermal, oil-gland, and HF differentiation. Using gain- and loss-of-function in vitro, we further implicate miR-125b as a repressor of SC differentiation. In vivo, transcripts repressed upon miR-125b induction are enriched >700% for predicted miR-125b targets normally downregulated upon SC-lineage commitment. We verify some of these miR-125b targets, and show that *Blimp1* and *VDR* in particular can account for many tissue imbalances we see when miR-125b is deregulated.

INTRODUCTION

Stem cells (SCs) possess intrinsic long-term properties that enable them to self-renew and differentiate into the specialized cell types of the tissue in which they reside. They are the basis of tissue homeostasis, wound-repair, and likely tumor growth as well (Rossi et al., 2008; Weissman, 2000). Elucidating the transcriptional and posttranscriptional mechanisms that control these properties is essential for understanding the basic principles of animal development, as well as realizing their therapeutic potential for regenerative medicine.

One excellent system to study SCs is the mouse skin, where distinct populations of epithelial stem cells give rise to different tissue structures with distinct turnover rates. SCs within the innermost (basal) layer of the interfollicular epidermis (IFE) and hair follicle (HF) orifice (infundibulum) generate a stratified, terminally differentiated epidermis, which turns over at a relatively constant rate in adult mice. Sebaceous gland (SG) SCs within the junctional zone of the HF outer root sheath (ORS) generate proliferative precursors for the terminally differentiated sebocytes that secrete lubricating oil for the hair and skin surface (Horsley et al., 2006; Jensen et al., 2009; Snippert et al., 2010). Just below this zone is the "bulge," a niche for the infrequently cycling SCs that fuel the hair cycle (Blanpain and Fuchs, 2009; Hsu et al., 2011). During the growth phase (anagen), the HF below the bulge regenerates and produces hair for several weeks. The HF then triggers a rapid destructive phase (catagen), which is followed by a quiescent resting phase (telogen), which can last for weeks (Cotsarelis et al., 1990; Oshima et al., 2001; Taylor et al., 2000). HF-SCs in the bulge are typically slow cycling, but they are activated at the start of the growth phase. The earliest progeny are thought to be cells along the ORS, which progress to become the transit-amplifying (TA) matrix at the bulb of the HF. After a brief period of active proliferation, matrix cells then terminally differentiate into one of the six distinct layers of the hair shaft and its channel, the inner root sheath (IRS) (Blanpain and Fuchs, 2009).

IFE, SG, and HF SCs share certain features, which include their expression of transcription factor p63 and keratins K14 and K5, as well as their high levels of integrins, reflective of their adherence to the underlying basement membrane that is rich in extracellular matrix and growth factors. Their close relation is further evidenced by the fact that, upon injury, HF-SCs can give rise to IFE and SG progenitors (Blanpain et al., 2004; Claudinot et al., 2005; Horsley et al., 2006; Levy et al., 2005; Morris et al., 2004; Nowak et al., 2008; Tumbar et al., 2004), a feature also suggested for IFE SCs (Ito et al., 2007). However, bulge SCs are distinguished from other skin SCs by their expression of CD34, Lgr5, and K15, and in addition, a group of essential transcription factors (Sox9, Nfatc1, Tcf3, Tcf4, and Lhx2) (Blanpain and Fuchs, 2009). Most of these markers and the slow-cycling properties of bulge HF-SCs are already evident in neonatal mice prior to completion of HF and SG morphogenesis (Nowak et al., 2008).

Posttranscriptional regulation in skin is also important, as evidenced by recent studies on microRNAs (miRNAs), which typically dampen expression of proteins by inducing degradation or translational inhibition of their target mRNAs (Ambros, 2004; Bartel, 2004). Most of the evidence comes from *K14-Cre* mediated conditional loss-of-function studies on core components of the machinery that generates these small (20- to 24-nucleotide) noncoding regulatory RNAs (Andl et al., 2006; Yi and Fuchs,

2010; Yi et al., 2006, 2009). miRNAs have been cloned from embryonic epidermis and HFs, and temporal analyses at the tissue level suggest that they have distinct patterns of expression in these two epithelia (Yi et al., 2006, 2009). Of these, *miR-203* has been identified as an inhibitor of "stemness" in IFE, where it is thought to act by repressing p63 translation as cells commit to differentiate (Lena et al., 2008; Yi et al., 2008). Conversely, *miR-205* is expressed throughout epidermis, where it is thought to function by regulating Akt activity and guard against apoptosis (Yu et al., 2010). The functions of miRNAs in SG and HF SCs remain unexplored, although their significance is suggested by the evagination of hair buds lacking miRNAs (Andl et al., 2006; Yi et al., 2006, 2009) and by the severely restricted HF and SG development seen in the few *K14-Cre* X *Dicer* mutant mice that survive into neonatal life (Andl et al., 2006).

Given increasing roles of miRNAs in regulating embryonic and adult SCs (Crist and Buckingham, 2009; Delaloy et al., 2010; Guo et al., 2010; Hatfield et al., 2005; Li and Gregory, 2008; Zhao et al., 2010), the relevance of specific miRNAs to skin SC biology merited further exploration. In the present study, we generated miRNA signatures for four different populations of keratinocytes that possess proliferative capacity within postnatal day 4 (P4) skin. To accomplish this goal, we exploited their differential expression of integrins, K14 and Sox9. We were particularly interested in miRNAs upregulated in P4 GFP^{+} ORS cells from *Sox9GFP* transgenic mice, given that lineage tracing revealed that these cells not only give rise to the adult HF and SG SCs, but also contribute to long-term repair of IFE upon wounding (Nowak et al., 2008).

Through miRNA array analysis, we show that, surprisingly, the miRNA signature of the early *Sox9GFP*-expressing cells is closely related to that of IFE basal cells but strikingly different from non-bulge ORS or matrix. We focused on miR-125b as an miRNA that is strongly expressed in *Sox9* promoter-active cells, somewhat expressed in basal epidermal cells, and significantly downregulated in ORS and matrix. We show that by sustaining miR-125b throughout K14-expressing cells, the transition from stemness to committed progenitor is markedly retarded both in vivo and in vitro. The consequences in vivo are dire—a hyperthickened epidermis, enlarged SGs, and a failure to generate a hair coat—but are fully reversible upon restoring normal miR-125b regulation. We isolate and profile transcripts that are expressed by WT early bulge and nonbulge progeny but repressed when miR-125b is sustained in progeny. Interestingly, transcripts repressed upon miR-125b induction are >700% enriched for conserved predicted miR-125b targets, which are normally downregulated in early bulge SCs versus their immediate early progenies. This enabled us to hone in on two key genes encoding transcription factors Blimp1 and VDR. We show that both are bona fide miR-125b targets in skin and can account for many of the phenotypic abnormalities that we see.

RESULTS

Purification of Early Bulge Cells by Fluorescence-Activated Cell Sorting

Our purification scheme was based upon transgenic mice coexpressing *K14-RFP* and *Sox9-EGFP* (Supplemental Experimental Procedures). Despite some EGFP in suprabasal cells of the upper HF near the hair shaft, only the early ORS region encompassing the future bulge and junctional zones showed strong colabeling of EGFP/Sox9, α6 integrin, and RFP/K14, thereby providing specificity for what we hereafter refer to as "early bulge cells" (Figure 1A). After enzymatically separating epidermis and dermis (including HFs) and generating single-cell suspensions, we used FACS to fractionate populations containing early bulge cells (Early Bulge) (RFP^{hi}GFP^{hi}α6^{hi}Lin^{neg}), ORS cells excluding the early bulge region (RFP^{hi}GFP^{neg}α6^{hi}Lin^{neg}) (mostly ORS cells below the bulge), transit-amplifying matrix cells (Matrix) (RFP^{lo}GFP^{neg}α6^{lo}Lin^{neg}) and IFE basal cells (Basal) (RFP^{hi}α6^{hi}Lin^{neg}) (Figures 1A–1C).

Real-time PCR verified the efficacy of our strategy and lineage assignments (Figure 1D). As expected, *Sox9* mRNA levels were highest in the RFP^{hi}GFP^{hi}α6^{hi}Lin^{neg} cells. This population was also enriched for other early bulge SC markers, including *Nfatc1*, *Tcf3*, and *Lhx2* (Blanpain and Fuchs, 2009), as well as junctional zone markers, Lgr6 and Lrig1 (Figure 1D; Table S1). Consistent with their known expression patterns (Horsley et al., 2008; Blanpain and Fuchs, 2009), *Nfatc1* was downregulated in the nonbulge ORS population, while *Sox9*, *Tcf3*, *Lhx2*, and *Lgr5* persisted (Figure 1D; Table S1). By contrast, the IFE and infundibulum marker *Sca-1* was enriched in RFP^{hi}α6^{hi}Lin^{neg} basal cells, while matrix marker *Msx2* was prominent in the RFP^{lo}GFP^{neg}α6^{lo}Lin^{neg} pool. As negative controls, *c-kit* (melanocytes) was not detected, and *vimentin* (fibroblasts) was only found at low levels in the matrix fraction. Taken together, these results confirmed our designations of these populations and their purity.

Defining a miRNA Signature for Early Bulge Cells

To identify miRNAs that are preferentially expressed in each fluorescence-activated cell sorting (FACS)-purified fraction, we performed miRNA microarrays (Experimental Procedures). Two interesting observations emerged upon analyzing these data. First, unsupervised hierarchical clustering revealed that the miRNA profile of the early bulge fraction was more closely related to the epidermal than ORS or matrix fractions (Figure 2A). This was surprising because bulge and ORS share more transcriptional similarities than basal epidermis. Second, individual members of an miRNA family that possess a common "seed" sequence tended to exhibit similar expression patterns among different skin cell populations (Figure 2B). The coordinate expression of functionally related miRNAs suggested a possible means of reinforcing the regulation of key miRNA target genes for these SC populations.

We selected four miRNAs with divergent expression patterns—miR-125b, miR-24, miR-205, and miR-31—and employed Taqman probes to verify their expression by RT-PCR (Figure 2C). MiR-125b was notable for its strong enrichment in the early bulge fraction. In situ hybridization confirmed its localized expression in the upper ORS (Figures 2D and 2E).

MiR-125b was particularly interesting in that it is a mammalian ortholog of *C. elegans lin-4* miRNA, the first animal miRNA characterized. In *C. elegans*, *lin-4* targets *lin-14* and *lin-28* to regulate temporally dependent developmental programs (Lagos-Quintana et al., 2002; Lee et al., 1993; Moss et al., 1997; Wightman et al., 1993). The *lin-4(miR-125)-lin-28* regulation pair has been evolutionarily conserved and functions critically in mammalian

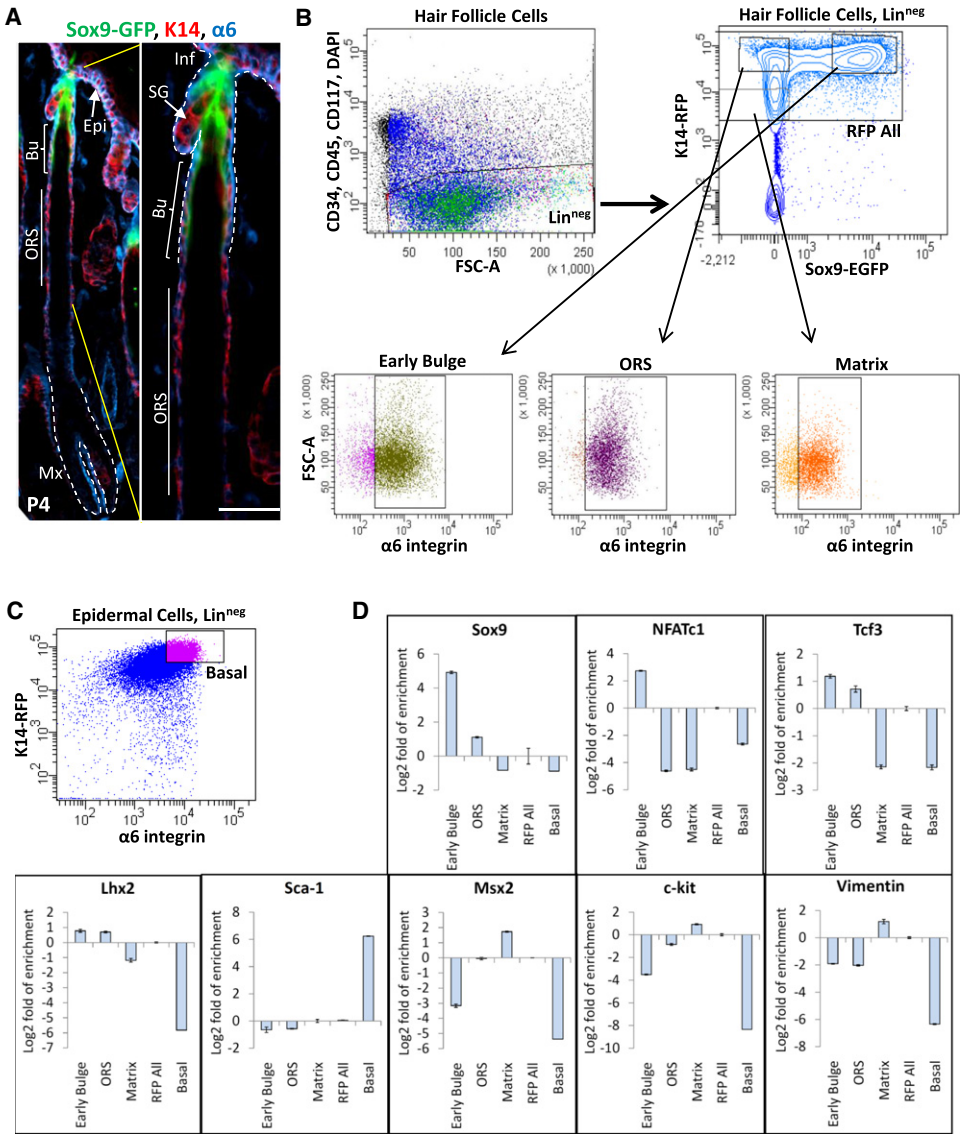

Figure 1. FACS Purifications of Backskin Populations Possessing Proliferative Capacity

Mice used are *K14-RFP/Sox9-EGFP* at P4.

(A) Immunofluorescence for markers used in purification. Bu, early bulge; ORS, non-bulge ORS; Mx, matrix; Epi, IFE basal layer; Inf, infundibulum; SG, sebaceous gland. Color coding is according to secondary antibodies (Abs) used. Scale bar represents 50 μm.

(B and C) FACS purifications. (B) HFs: RFP^{hi}GFP^{hi}α6^{hi}Lin^{neg} Early Bulge, RFP^{lo}GFP^{-}α6^{+}Lin^{neg} non-bulge ORS, RFP^{lo}GFP^{-}α6^{lo}Lin^{neg} Matrix, and RFP^{+}Lin^{neg} reference cells (RFP All). (C) IFE: RFP^{hi}α6^{hi}Lin^{neg} IFE (Basal).

(D) RT-PCR. Vertical axis represents Log2-transformed Fold of enrichment comparing with the RFP-All reference population. Error bars represent standard error. GAPDH was used as a reference gene for all RT-PCR.

See also Table S1.

embryonic SC differentiation (Rybak et al., 2008; Wu and Belasco, 2005). miR-125b's localization in the upper ORS made it a candidate for regulating early bulge SCs. However, because *lin-28* was not expressed in postembryonic skin, miR-125b must control other targets in the HF.

Maintaining miR-125b in Skin SC Progeny Causes Striking Pleiotropic Phenotypes

To explore miR-125b's role in skin SCs, we first devised a strategy to sustain its expression in nonbulge ORS, where it is normally downregulated, and to upregulate it in basal epidermal cells, where it is normally expressed at lower levels than in bulge. For this purpose, we engineered three lines of transgenic mice to express miR-125b under the control of a tetracycline regulatory element (TRE) (Figure 3A). The TRE-miR-125b mice were then mated with our previously described transgenic line that expresses the tetracycline-sensitive transactivator, rtTA2S-M2-VP16 (rtTA), controlled by a *keratin 14* (K14) promoter that is active in ORS and basal epidermis (Nguyen et al., 2006). Within 24 hr after tetracycline (doxycycline, Dox)

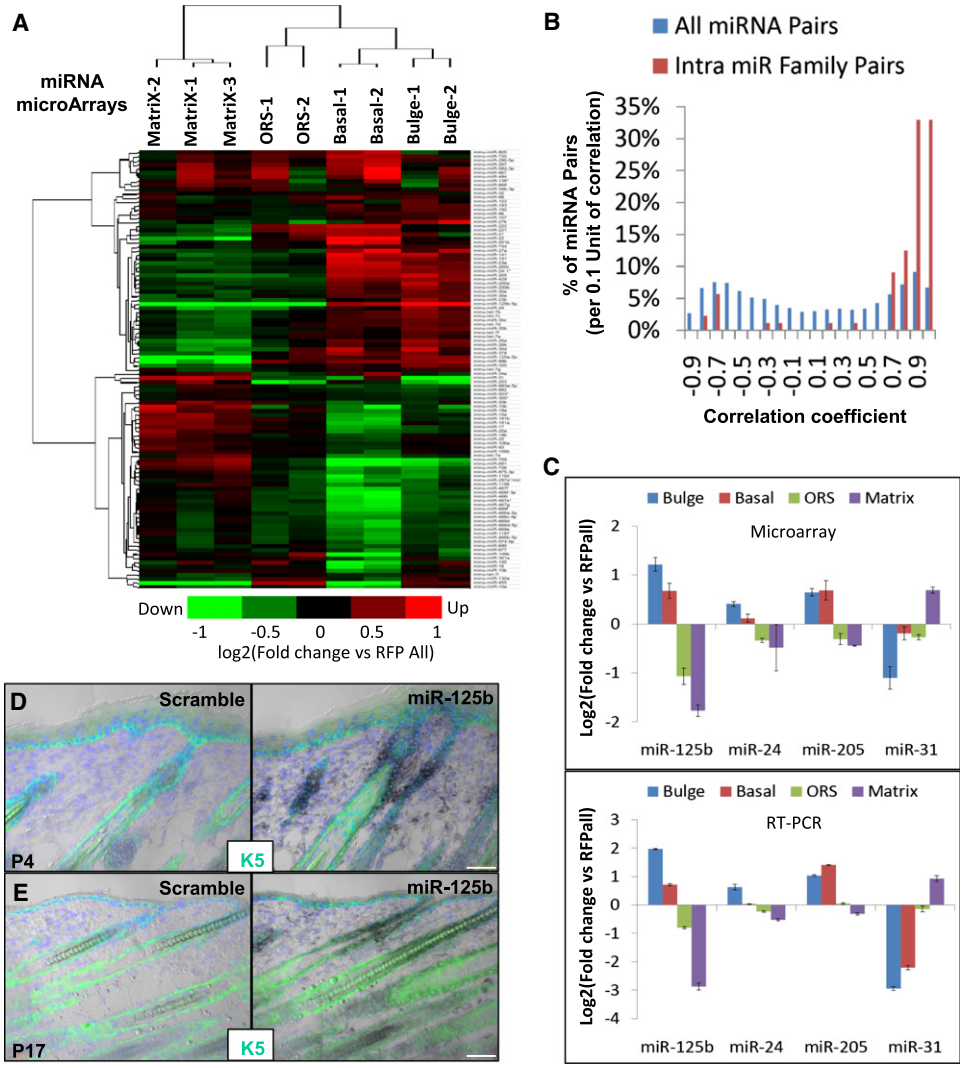

Figure 2. Differential Expression of miRNAs

(A) Unsupervised hierarchical clustering and heat map display of miRNA expression profiles of FACS-purified populations. Comparisons are normalized to the RFP-All reference cell population. Each row represents an individual miRNA. Each column represents an independent sample. Two to three biological replicates were analyzed for each population. Red represents downregulation, while green represents upregulation compared to RFP-All.

(B) Histogram of Pearson's correlation coefficient of expression patterns between all possible miRNAs (blue bars) or between miRNAs that belong to the same miRNA family (intrafamily, red bars). The correlation of expression was calculated based on the miRNA expression profiles presented in (A).

(C) miRNA-microarray results and RT-PCR verification of expression patterns of the miRs indicated. U6 was used as the reference gene in RT-PCR. Error bars represent standard error.

(D and E) miR-125b in situ hybridizations of WT P4 and P17 backskins. In situ signals (black) were developed by BM purple substrate: K5 (green) in ORS and basal IFE. Scale bars represent 50 μm.

induction, *K14-rtTA/TRE-miR-125b* double transgenic mice (DTG) exhibited robust miR-125b expression in all K14(+) cells, including basal epidermis and ORS (Figure 3B). MiR-125b induction was confirmed by RT-PCR on FACS-isolated DTG ORS cells (Experimental Procedures). Strong and specific induction of miR-125b was observed without significant disturbance of other unrelated miRNAs (Figure 3C).

Without Dox, the mice developed normally and were morphologically indistinguishable from wild-type (WT) littermates (Figure 3D). When Dox was administered to neonatal mice during the growth phase of the first hair coat (P3), hair growth was inhibited, a feature which became obvious 10 days later (Figure 3D). When Dox was given during the first resting phase (P21) and then monitored through one entire hair cycle to the second resting phase (P48), the new hair coat never emerged (Figure 3D). As long as miR-125b was sustained, baldness persisted. All three DTG lines behaved analogously, although the progression to baldness varied among them, likely reflective of their different miR-125b expression levels (Figure S1).

Hair growth inhibition was best visualized by administering Dox at P56 during the prolonged telogen phase of the 2nd postnatal hair cycle, and then waxing backskins 2 days later to

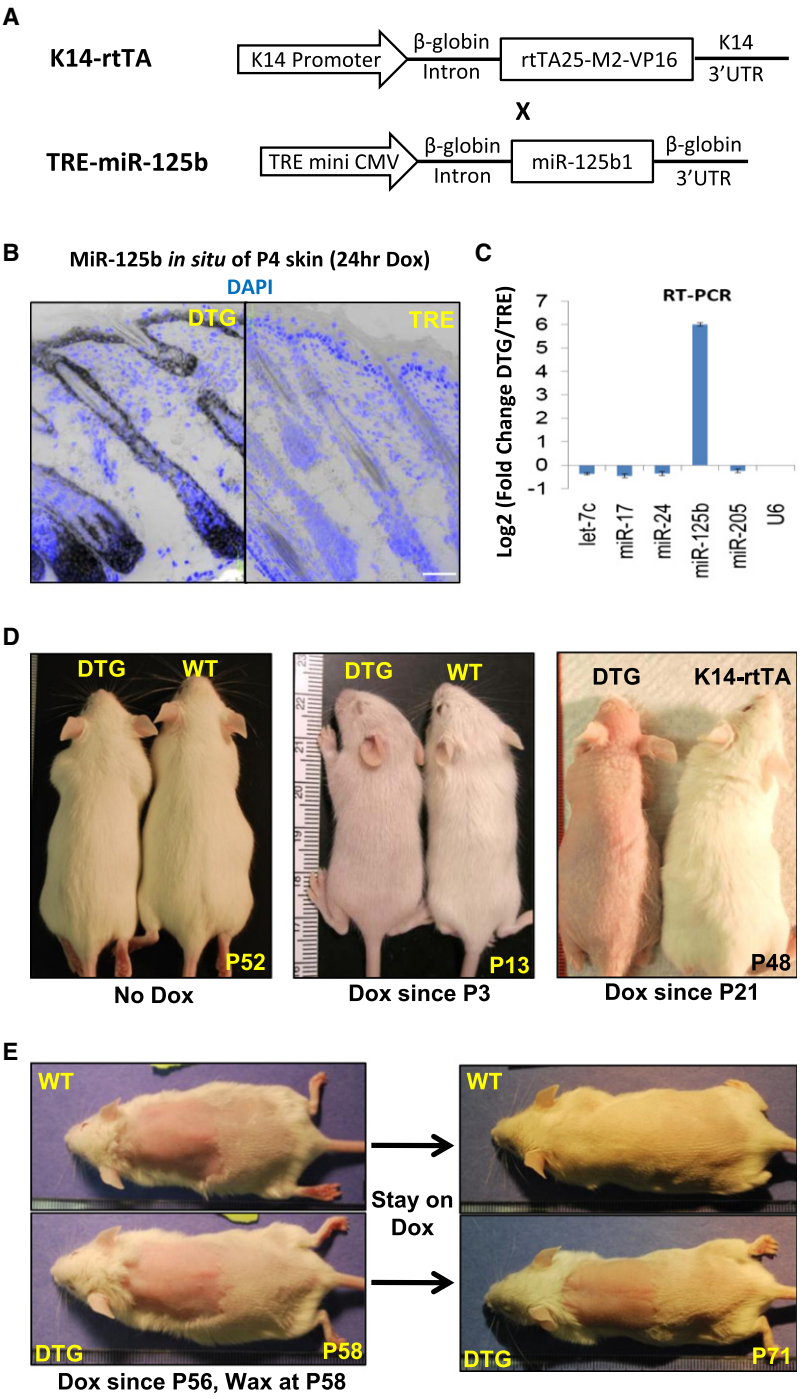

Figure 3. Sustained miR-125b Blocks Hair Growth

(A) Schematic of constructs used to generate DTG mice.

(B) miR-125b in situ hybridizations of P4 backskin sections harvested after 24 hr Dox induction. In situ signal, black; DAPI, blue; TRE, TRE-miR-125b single transgenic; DTG, double transgenic. Scale bar represents 50 μm. Note that high miR-125b levels are no longer confined to HF-SCs but are now expanded to early progeny.

(C) Taqman RT-PCR analysis of miRNAs in FACS-sorted P4 stage backskin ORS cells. Error bars represent standard error.

(D) Appearance of DTG and WT littermates given Dox at P3 (anagen) or P21 (telogen) and photographed at ages indicated.

(E) Mice were given Dox at P56, and at P58, the upper backskins were waxed and lower parts were shaved. Animals were photographed at ages indicated.

See also Figures S1 and S2.

eliminate existing club hairs and promote precocious, synchronous initiation of a new hair cycle. In WT mice, the coat regrew in the depilated area by P71, while miR-125b-induced mice still displayed the bald patch (Figure 3E). Intriguingly, while hair growth was markedly impaired in DTG mice, growth of some other skin tissues and appendages was noticeably accentuated. This was particularly true for the lips, nails, and anogenital areas in which the *K14* promoter is active (Figures S2A and S2B). Moreover, when Dox was administered to DTG mice, the hair coat became greasy prior to its loss. Closer inspection revealed greatly enlarged SGs, whose sebocytes stain with oil red O (Figure 4A).

MiR-125b Regulates SG Development By Targeting Blimp1 Through a Conserved 3′UTR Binding Site

The enlarged SGs accompanying miR-125b induction were reminiscent of those in mice conditionally targeted for *Blimp1,* which encodes a transcriptional repressor normally expressed by *K14*-promoter-active sebocyte progenitors (Horsley et al., 2006). Indeed, immunofluorescence microscopy revealed a marked reduction in Blimp1 protein following induction of miR-125b (Figure 4B). RT-PCR confirmed that *Blimp1* mRNA levels were also strongly downregulated in Dox-induced DTG skin. Analogous to the *Blimp1* cKO animals, the sebocyte marker *PPARγ* was strongly upregulated (Figure 4C).

The 3′UTR of *Blimp1* mRNA is predicted by TargetScan (Lewis et al., 2005) to contain a single miR-125b binding site that is well conserved from amphibian to mammals. To test the hypothesis that *Blimp1* mRNA may be a direct target of miR-125b in skin, we constructed a luciferase reporter for WT *Blimp1* 3′UTR, as well as a control reporter in which the miR-125b binding site of the *Blimp1* 3′UTR was mutated (Figure 4D). Luciferase reporter assays were then carried out in primary keratinocytes (MK) cultured from P0 epidermis of WT skin and transfected with synthesized miR-125b precursor (Pre-miR-125b) or control Pre-miR.

Elevated miR-125b resulted in strong repression of the WT *Blimp1* 3′UTR reporter, but not a mutant *Blimp1* 3′UTR reporter lacking the miR-125b binding site (Figure 4E). Furthermore, when miR-125b was repressed by transfecting antisense LNA probes against miR-125b into cultured MK, WT *Blimp1* 3′UTR

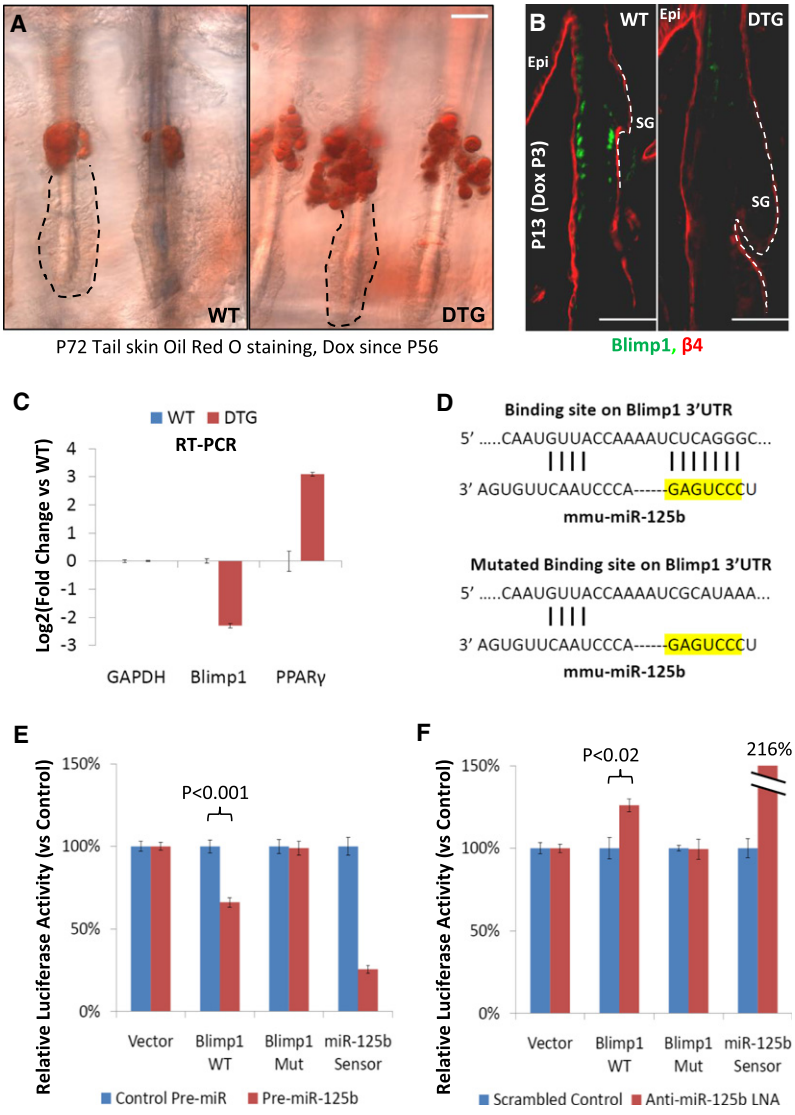

Figure 4. Enlarged Sebaceous Glands in DTG Mice Traced to miR-125b-Induced Suppression of *Blimp1*

(A) Whole-mount Oil Red O staining of tail skin of P72 DTG and WT littermates (+Dox a/P56).

(B) Anti-Blimp1 immunofluorescence of backskin sections of P13 mice (+Dox a/P3).

(C) RT-PCR of P79 tail skin mRNAs of P79 mice (+Dox a/P21). GAPDH, reference.

(D) Pairing between predicted miR-125b binding site on Blimp1 3′UTR and mmu-miR-125b. The seed region of miR-125b is highlighted.

(E and F) Relative luciferase activity of WT and Mutated (Mut) Blimp1 3′UTR reporters in cultured MK when cotransfected with pre-miRNA precursors (E) or antisense LNA knockdown probes (F) compared with their corresponding controls. The vector control is CMV-PGL4. The effectiveness of miR-125b overexpression by pre-miR-125b precursor and miR-125b knockdown by anti-miR-125b LNA was confirmed by the activity of miR-125b sensor.

All error bars represent standard error unless otherwise indicated. All scale bars represent 50 μm unless otherwise indicated.

reporter activity was significantly upregulated in contrast to the control reporter (Figure 4F). Taken together, these data indicate that *Blimp1* mRNA is a direct and functionally relevant target of miR-125b in skin keratinocytes.

MiR-125b Represses Hair Differentiation

While the link between miR-125b and Blimp1 was sufficient to account for the SG phenotype, it did not explain the hair growth defect observed in our mice. To decipher how sustained miR-125b expression might induce baldness, we first examined backskin histology from strain-, sex- and age-matched littermates of Dox-induced DTG versus WT (or single transgenic) mice. Surprisingly, near the end of the first anagen, when WT littermate HFs had reached maximal length (P13, Dox-induced since P3), DTG HFs were much longer, exhibiting a highly elongated ORS (Figure 5A). Immunofluorescence microscopy showed proper expression of ORS markers K14 and β4 integrin but a marked reduction in markers of matrix-derived hair shaft and inner root sheath (IRS) cells (Figure 5B).

The dearth of hair shaft and IRS cells could arise from repressed terminal differentiation, an increase in cell death, or an impaired ability of matrix to fuel production of these lineages. To distinguish between these possibilities, we examined matrix size and proliferative potential. When P13 mice were pulsed by a single injection with the nucleotide analog BrdU and sampled after 4 hr, S phase cells were primarily in matrix (Figure 5C). Compared to WT, DTG HFs showed a >30% reduction in labeled matrix cells. By 11 hr, many of these labeled cells in WT HFs had moved into the nondividing precortex, reflecting their normal progression of differentiation. By contrast, an ~3× reduction was seen in labeled DTG precortical cells (Figure 5C). Taken together, these data revealed reductions both in the number of dividing transiently amplifying (TA) cells in the matrix and their rate of differentiation into hair shaft and IRS lineages.

The underlying basis for these lineage defects did not appear to reside in enhanced cell death (apoptosis), as evidenced by the relative lack of activated caspase 3 staining, except for the core of the hair shaft, also positive in WT HFs (Figure 5D). We therefore focused on earlier steps along the lineage, namely in the progression of activated HF-SC progeny along the ORS to matrix. Further analysis of $BrdU^+$ cells revealed a modest reduction in labeled cells within the lower DTG ORS during both 4 hr and 11 hr labeling periods (Figure 5E). Unexpectedly however, the upper ORS, including the bulge region, showed an ~6- to 7× enhancement in S phase cells in these HFs (Figure 5F). This was accompanied by hyperthickening of this zone (Figure 5G), a feature not seen in mid and lower ORS (Figure 5B). Taken together with the marked elongation of the mid/lower DTG ORS, these data suggest that sustained miR-125b in the ORS increases the number of cell divisions that early bulge cells

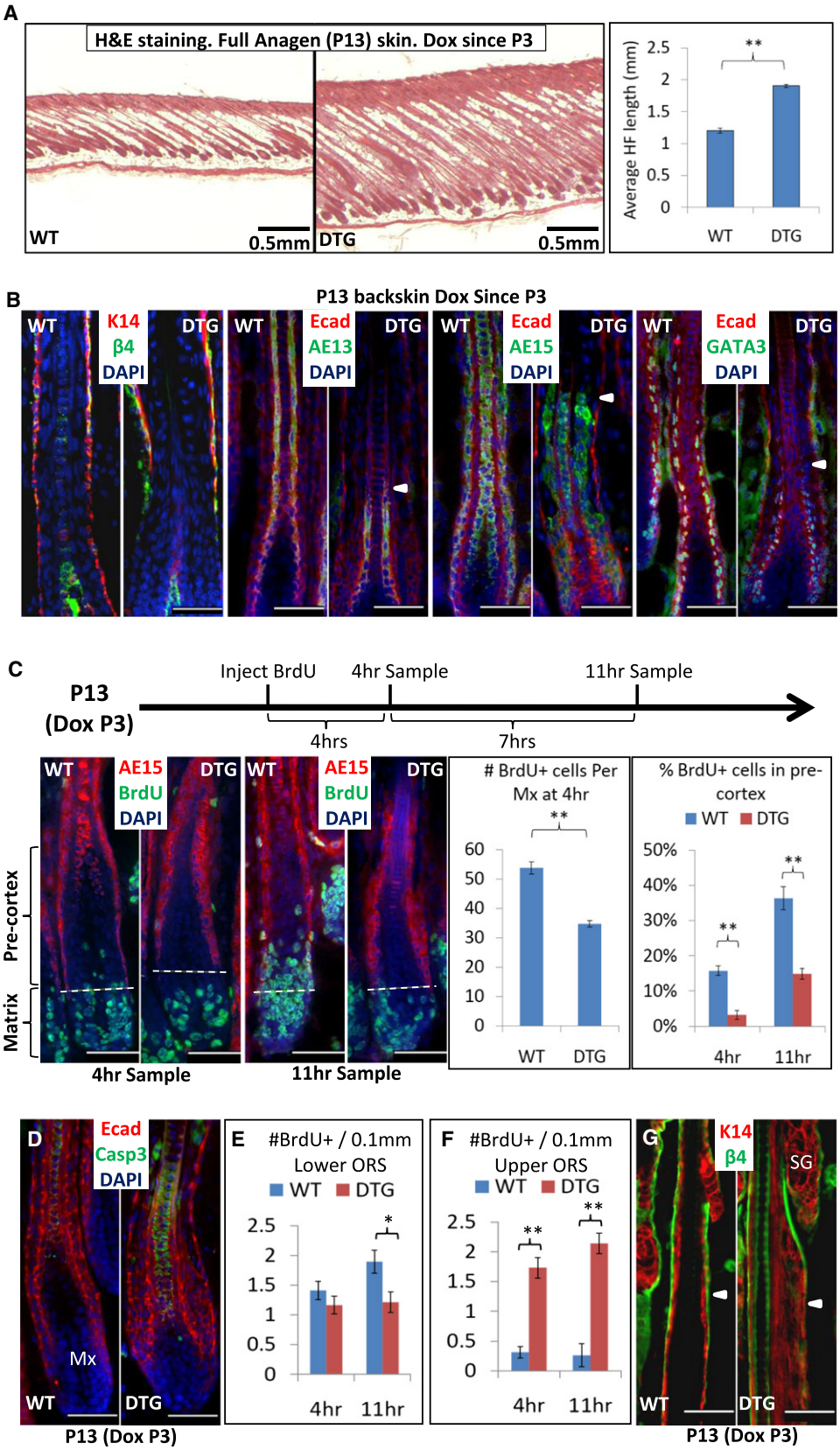
A
H&E staining. Full Anagen (P13) skin. Dox since P3
WT
0.5mm
DTG
0.5mm
Average HF length (mm)
2.5
2
1.5
1
0.5
0
**
WT
DTG
B
P13 backskin Dox Since P3
WT
K14
β4
DAPI
DTG
WT
Ecad
AE13
DAPI
DTG
WT
Ecad
AE15
DAPI
DTG
WT
Ecad
GATA3
DAPI
DTG
C
P13
(Dox P3)
Inject BrdU
4hr Sample
11hr Sample
4hrs
7hrs
WT
AE15
BrdU
DAPI
DTG
WT
AE15
BrdU
DAPI
DTG
Pre-cortex
Matrix
4hr Sample
11hr Sample
BrdU+ cells Per Mx at 4hr
**
60
50
40
30
20
10
0
WT
DTG
% BrdU+ cells in pre-cortex
WT
DTG
50%
40%
30%
20%
10%
0%
**
**
4hr
11hr
D
Ecad
Casp3
DAPI
Mx
WT
DTG
P13 (Dox P3)
E
#BrdU+ / 0.1mm
Lower ORS
WT
DTG
2.5
2
1.5
1
0.5
0
*
4hr
11hr
F
#BrdU+ / 0.1mm
Upper ORS
WT
DTG
2.5
2
1.5
1
0.5
0
**
**
4hr
11hr
G
K14
β4
SG
WT
DTG
P13 (Dox P3)

and/or their progenitors make, which in turn restricts their commitment and progression along the lineage.

MiR-125b Inhibits the Differentiation of Skin SCs Without Affecting Their Maintenance or Activation

Thus far, our data suggested that stemness may still be maintained when miR-125b cannot be downregulated in HF-SC progenies. To examine this possibility, we first looked at bulge markers Lhx2, Sox9, Tcf4, Nfatc1, and CD34 in Dox-induced DTG skins of adult mice. With the exception of CD34, all these markers were still present 17 days after miR-125b induction (Figure 6A; Figure S3). To determine whether DTG skin still possessed functional HF-SCs, we administered Dox at P21, waited until DTG mice were bald at P58, and then either kept mice on Dox or withdrew Dox until P94. For comparative purposes, an area of skin from WT mice was shaved so we could monitor hair regeneration.

The results of the experiment are shown in Figure 6B. As expected, only WT mice grew their hair when Dox was maintained. Interestingly however, by 5 week after Dox withdrawal, DTG hair coats had largely regenerated. This happened even when mice were kept on Dox for 4 months prior to withdrawal (data not shown). Since the hairless phenotype was reversible, the defect appeared to be a delay in the rate of bulge→hair lineage progression rather than a loss of HF-SCs.

To determine whether sustained miR-125b prevented HF-SC activation, we stimulated resting (telogen-phase) HFs by depilation (waxing) to initiate a new hair cycle and then examined the response by administering a 48 hr pulse of BrdU. Under these conditions, >50% of Sox9$^+$ cells in both WT and Dox-induced DTG HFs showed active cycling (Figure 6C). Moreover, signs of a Sox9(−) early matrix were also apparent at this time. Thus, even though hair coat formation was impaired in Dox-induced DTG mice (Figure 3E), HF-SCs were still able to respond to a hair growth stimulus.

If miR-125b inhibits hair lineage differentiation without impairing the maintenance and activation of the HF-SCs, then either relatively undifferentiated SC-derived progeny and/or HF-SCs themselves should accumulate in DTG HFs after Dox induction. To test this hypothesis, we FACS-purified and cultured equivalent numbers of ORS cells from HFs of DTG and control mice and compared their ability to form large (>2 mm) colonies (holoclones), a characteristic of skin SCs (Barrandon and Green, 1987). Holoclone-forming efficiency was at least 3× higher in ORS cells isolated from induced DTG versus WT HFs (Figure 6D). Moreover, >30% of holoclones formed by DTG ORS cells could be serially passaged >3× in culture, a characteristic of adult bulge HF-SCs, but not their progeny (Greco et al., 2009) (Figure 6E). The difference in holoclone numbers was not attributable to differences in cell attachment but, rather, to enhanced colony initiation efficiency (where a colony is defined as ≥4 cells) (Figures 6F and 6G).

The increased ability of DTG ORS to generate holoclones could either reflect an expanded HF-SC pool or, alternatively, an increase in the proliferation rate of early bulge progeny. To distinguish between these possibilities, we overexpressed miR-125b in cultured WT MK, which resulted in a significant decline in both overall proliferation rate and the percentage of S phase cells (Figure S4). Thus while the DTG ORS contained a higher percentage of cells with holoclone forming and passaging ability, elevated miR-125b in vitro made cells grow more slowly. Together, these findings suggest that miR-125b's function resides in enhancing SC self-renewal rather than promoting proliferation in general.

The effects of miR-125b on SC behavior extended to IFE progenitors. In vivo, the IFE of Dox-induced DTG skin was hyperthickened, and signs of basal cell expansion were evident (Figure 6H). In vitro, cultured MK from DTG versus WT epidermis displayed a significantly dampened response to calcium-induced terminal differentiation when exposed to Dox (Figure 6I). Conversely, when exposed to an antagomIR specific for miR-125b, WT epidermal cells displayed an accentuated response to calcium-induced differentiation (Figure 6J).

Identification of Additional miR-125b Target Genes

miRNAs often downregulate the mRNA level of their target genes (Baek et al., 2008; Lim et al., 2005; Selbach et al., 2008). Therefore, to gain further mechanistic insights underlying miR-125b's effects, we conducted microarray analysis on ORS cells from P4 WT and DTG mice that had been treated with Dox 1 day earlier. We conducted our analyses on independent, duplicate matched sets of male and female mice.

miRNAs only modestly regulate their target mRNA levels (Baek et al., 2008; Selbach et al., 2008), and our aim was to identify early changes occurring shortly after miR-125b induction. Hence, we chose a relatively modest cutoff, Log2(DTG/Control Fold of change) < −0.3, for scoring a gene as being downregulated in each array. Notably however, under this criterion, TargetScan-predicted, conserved miR-125b targets were prominent within the downregulated genes of both datasets (Figure S5). Moreover, the DIANA-mirExTra algorithm (Alexiou et al. 2010) identified miR-125b's seed sequence "CUCAGG" as the most overrepresented, conserved hexamer motif within 3′UTRs of these downregulated genes. Thus, our strategy to

Figure 5. Repressed Differentiation and Expansion of Early Bulge ORS Region in DTG HFs

DTG and WT littermates were treated with Dox a/P3 and backskin sections were either examined at P13 (A and B) unless subjected to further experimentation (C-G).

(A) Hematoxylin and eosin staining and quantification of average HF length.

(B) Immunofluorescence for ORS, IRS, and hair shaft markers.

(C) Schematic of BrdU experiment. Immunofluorescence with Abs indicated (color coding according to secondary Abs). Quantifications: number of BrdU$^+$ cells per matrix (section) 4 hrs a/BrdU; percent of BrdU$^+$ cells in precortex (early hair shaft) region and IRS at times indicated a/BrdU.

(D) Immunostaining for activated caspase 3 shows little or no change in DTG versus WT littermate.

(E and F) Quantifications of BrdU$^+$ cells in lower versus upper ORS.

(G) Immunofluorescence reveals hyperthickened upper ORS bulge region in DTG HF.

All error bars represent standard error unless otherwise indicated. All scale bars represent 50 μm unless otherwise indicated.

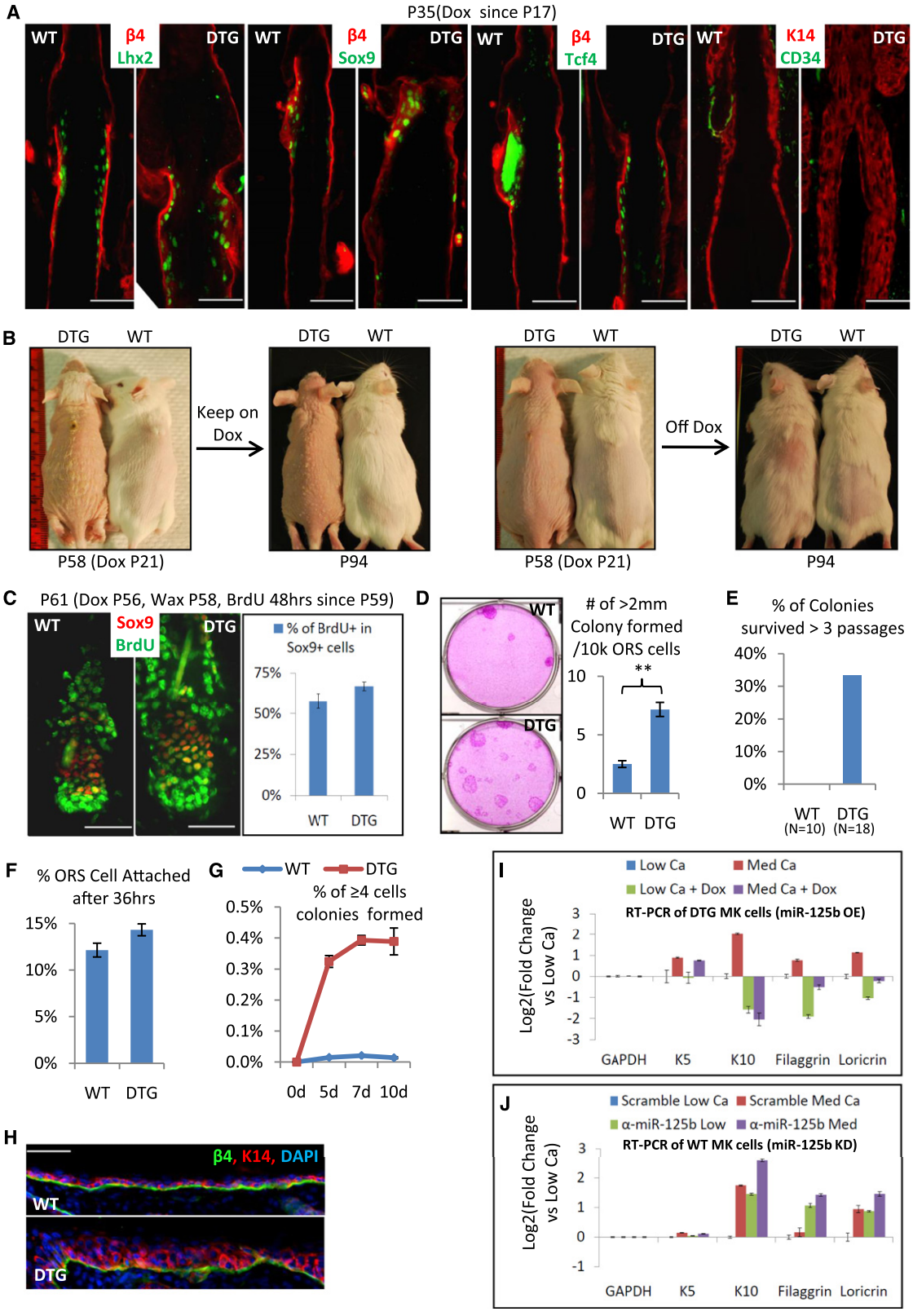

Figure 6. Evidence for Expansion of Stem Cell Populations in DTG Skin

(A) Immunofluorescence reveals presence of some, but not all, HF-SC markers in DTG skin (Dox a/P17; analyses a/P35).

(B) Hair coat recovery after Dox withdrawal in DTG mice. Mice were given Dox a/P21; a/P58, Dox was either continued or withdrawn as indicated.

detect miR-125b targets was yielding meaningful specificity and sensitivity.

Because sustained miR-125b resulted in analogous HF phenotypes in male and female mice, we reasoned that the majority of bona fide miR-125b targets in ORS cells should be downregulated in both sexes. Consistent with this idea, ~12% of genes scoring as downregulated in both sexes upon miR-125b induction displayed conserved miR-125b binding sites in their 3′UTRs (Figure 7A). This represented an ~6× enrichment compared to that of all ORS-expressed genes and an ~3× enrichment compared to that of genes downregulated in either sex alone. This indicated that the specificity for miR-125b target detection would be greatly improved by focusing on the overlap in downregulated genes in our two datasets. Hereafter, we refer to these genes as "miR-125b downregulated genes" (Table S2).

Expression of a miRNA often inversely correlates with that of its targets (Farh et al., 2005; Stark et al., 2005). Because miR-125b is naturally enriched in early bulge but strongly downregulated in nonbulge ORS, we posited that physiologically relevant miR-125b target mRNAs should be expressed at reduced levels in early bulge compared with nonbulge ORS. To explore this possibility, we performed microarray analyses on mRNAs isolated from our FACS-purified early bulge and nonbulge ORS populations of P4 stage backskin HFs. Interestingly, when WT early bulge transcripts were compared with those in ORS, mRNAs that scored as being preferentially downregulated in WT early bulge encompassed many mRNAs that were also downregulated in miR-125b-induced DTG ORS (Figure 7B). These data suggest that a significant portion of miR-125b-downregulated genes in the DTG ORS are endogenous miR-125b targets in WT early bulge cells.

Thus far, our data revealed that miR-125b downregulated genes were significantly enriched for both Targetscan-predicted miR-125b targets and also downregulated genes in WT early bulge versus non-bulge ORS. Remarkably, the highest enrichment (>700%) was observed for predicted conserved miR-125b targets that were also downregulated naturally in miR-125b$^+$ early bulge versus miR-125b(−) nonbulge ORS (Figure 7C). To derive a list of high-confidence potential miR-125b targets, we overlapped these criteria and identified those miR-125b downregulated genes that also (1) show downregulation in WT early bulge compared to nonbulge ORS cells and (2) possess at least one Targetscan-predicted conserved miR-125b binding site in the 3′UTR. By applying these criteria, we generated a short-list of 33 genes as putative miR-125b targets in the early bulge region (Table S3). From this list, we picked three potentially interestingly targets for further verification: *Vdr* encodes VDR (vitamin D receptor), involved in HF differentiation; *Trp53Inp1* encodes a positive regulator of a known miR-125b target, p53; and *Scarb1* harbors two conserved miR-125b binding sites in the 3′UTR. We validated their miR-125b binding sites by luciferase reporter assays (Figure 7D).

MiR-125b Regulates Hair Differentiation by Repressing VDR Expression

We focused on *Vdr* because it is required for HF differentiation (Palmer et al., 2008) and its loss results in a hairless phenotype (Li et al., 1997). Our microarray data revealed higher levels of *Vdr* (~1.7×) in nonbulge ORS than in early bulge ORS, and this was confirmed by immunofluorescence microscopy (Figure 7E). In DTG ORS, VDR expression was markedly diminished, and transcripts of genes previously identified as putative HF targets for the VDR transcription factor (Palmer et al., 2008) were significantly downregulated both in DTG tail skin and in purified ORS cells (Figures 7E–7H).

We confirmed the negative regulation of miR-125b on the activity of VDR pathway by testing a VDR-responsive element (VDRE) luciferase reporter construct in cultured DTG MK. When miR-125b expression was induced by Dox, the expression of the VDRE reporter in response to the Vitamin D Analog EB1089 (Palmer et al., 2008) was dramatically reduced (Figure 7I). Conversely, in cultured WT MK, anti-miR-125b antagomir treatment significantly enhanced VDRE reporter expression in response to EB1089 (Figure 7J).

Finally, if the downregulation of VDR pathway activity contributes to the miR-125b-dependent inhibition of hair differentiation, stimulation of the pathway by ectopic VDR ligand should dampen the phenotype. Consistent with this hypothesis, IP injection of EB1089 partially rescued the hair growth defect in DTG mice during depilation (waxing)-initiated hair cycle (Figure 7K). Similar rescue effects were achieved via topical application of EB1089 solution (Figure S6).

DISCUSSION

A miRNA Signature of "Stemness" in the Hair Follicle

In the present study, we identified a miRNA expression signature which specifically associates with stemness in HFs, and at least for miR-125b, this signature is functionally relevant to tissue homeostasis. It is tempting to speculate that by coordinately fine-tuning the expression of a large number of proteins, miRNAs may confer greater accuracy than transcription factors in acting

(C) HF-SCs are activated comparably in DTG and WT by wax-induced depilation of resting phase follicles. BrdU was administered beginning 1 day a/waxing and HFs were analyzed and quantified 2 days later.
(D and E) 10^4 FACS sorted ORS cells from Dox-induced P33 DTG and WT littermates were plated and after 2 weeks, cultures were either fixed and stained (D) or individual large clones were picked, serially passaged, and quantified for long-term survival (E). Note: WT bulge cell colonies typically have <10% survival rate in serial passage experiments (Greco et al., 2009), and WT ORS consists of bulge and nonbulge ORS. DTG ORS is highly enriched for holoclones.
(F and G) FACS sorted ORS cells from P59 K14H2BGFP DTG and WT HFs (Dox a/P21) attach comparably 36 hr a/plating onto feeder-coated dishes, but colony-forming efficiency is higher for DTG cells.
(H) Immunofluorescence reveals expansion of basal cells in IFE of P13 DTG backskin (Dox a/P3).
(I and J) RT-PCR for basal versus differentiation markers. mRNAs were from MKs in either low Ca^{2+} (0.05 nM) media or a/switching to medium Ca^{2+} (0.3nM) media for 24 hr. (I), DTG MK ± Dox induction as indicated. (J), WT MK treated with anti-miR-125b or control scramble antagomirs as indicated.
All error bars represent standard error unless otherwise indicated. All scale bars represent 50 μm unless otherwise indicated.
See also Figures S3 and S4.

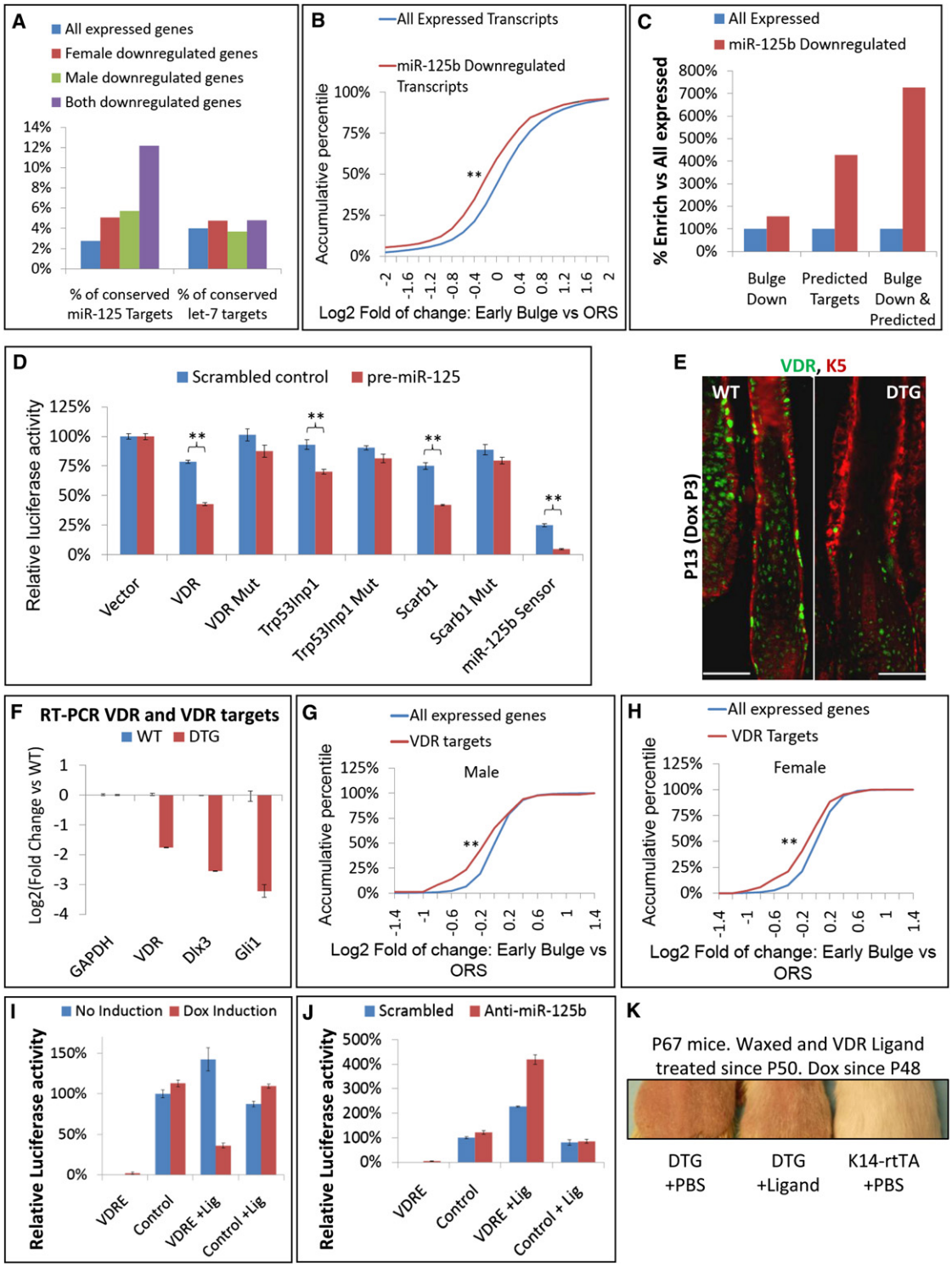

Figure 7. Identifying and Testing Putative miR-125 Targets in Skin SCs

(A) mRNAs from DTG versus WT ORS from P4 male and female mice were subjected to microarray analyses to identify a list of mRNAs downregulated by miR-125b (see text). Shown are the percentages (%) of predicted targets for miR-125b and let-7 among the list.

(B) mRNAs from P4 WT early bulge and non-bulge ORS were subjected to microarray analyses. Shown is an accumulative percentile map for the distribution of the miR-125b downregulated genes from (A) within these new array data.

(C) Comparisons reveal that miR-125b downregulated genes tend to be downregulated in early bulge versus nonbulge ORS.

(D) Luciferase reporter assays validate the predicted conserved miR-125b binding sites in the 3′UTRs of 3 miR-125b downregulated ORS genes. Mut indicates constructs with mutated miR-125b binding sites.

as a rheostat to regulate decisions involving the switch from stemness and commitment (Stark et al., 2005).

In the hair lineage, quiescent bulge SCs are known to be activated by external Wnt promoting and BMP inhibitory signals. As progeny move downward along the ORS, they are thought to progressively adjust their fate from that of SCs to committed progenitors. Eventually, these cells will pass a point of no return and end up as TA matrix (Hsu et al., 2011). The dramatic switch in miRNA expression profile between early bulge and nonbulge ORS and the similarities between ORS and matrix miRNAs suggest that miRNAs may function in regulating fate progression through this transition point. In this regard, it was particularly interesting that miR-125b exhibited a sharp downregulation early in the lineage between bulge and adjacent ORS. Moreover, when this switch was blocked by enforcing miR-125b expression throughout the ORS, a gross distortion arose in the relative ratios of cells with stemlike characteristics and those further along the hair lineage. Notably, miR-125b did not seem to affect the maintenance, self-renewing ability, or activation of HF-SCs.

Within the DTG HF lineage, the upper ORS region was hyperthickened, while mid/lower ORS was merely elongated and the progression to a TA cell fate was actually delayed. Given the absence of defects in bulge SC maintenance or activation, our findings best suit a model whereby miR-125b acts as a rheostat whose downregulation controls the rate at which bulge progenies transit through the commitment step along the lineage. This view is further supported by the dramatic miR-125b-dependent increase in holoclone-forming cells within the ORS (including bulge). Importantly, miR-125b does not promote proliferation per se, because when miR-125b is overexpressed in vitro, cells grow at a significantly slower rate.

When our in vivo and in vitro data are taken together, they point to a role for high miR-125b as a faithful definer of self-renewing, slow-cycling SCs, while reducing miR-125b was required to transition to a state of rapid proliferation, fate commitment, and differentiation. Our results help to explain a myriad of seemingly paradoxical findings about miR-125b, where in some cell types, it has been reported to be an oncomir and in others, a tumor suppressor. Our studies show how miR-125b can suppress overall proliferation while still acting to expand stem cell numbers and tissue/organ size.

miR-125: A Global Balancer of Stemness and Commitment in Adult Tissues?

Another key finding was that miR-125b's rheostat function in governing the switch between stemness and commitment was not limited to the HF lineage. In the normal IFE, which also modestly expresses miR-125b in the basal layer, miR-125b elevation resulted in an expansion in the number of layers possessing features of undifferentiated cells in vivo. Moreover in cultured epidermal MK, calcium-induced differentiation was enhanced when miR-125b was knocked down and repressed when miR-125b was elevated. Finally, because Blimp1 is known to limit SG progenitors by repressing c-Myc (Horsley et al., 2006), miR125b's ability to repress Blimp1 and yield enlarged SGs was likely rooted in an expansion of its progenitors.

In B cells, Blimp1 has been reported to induce differentiation (Turner et al., 1994). Moreover, in vitro studies recently showed that overexpression of miR-125b leads to Blimp1 repression and inhibition of B cell differentiation (Gururajan et al., 2010; Malumbres et al., 2009). One model that could explain these seemingly paradoxical effects of Blimp1 in the SG versus B cell lineages is that by downregulating Blimp1 in SG progenitors, miR125b makes the cells go through extra rounds of proliferation before they can progress into a more differentiated cell fate. This would effectively delay differentiation and expand the pool of less differentiated SG cells.

This same logic can potentially be applied to other lineages. When the differentiation process is delayed and/or repressed by miR-125b, actively cycling undifferentiated progenitors will accumulate, generating an enlarged tissue/organ, as seen for the lips, anogenital epithelium, nails, ORS, and epidermis in our miR-125b-induced mice. This would also explain why in epidermis, ORS, and SG, the most dramatic changes in proliferation seen in Dox-induced DTG skin occurred at the juncture between SCs and their immediate progeny. Notably, this is also the site of dramatic downregulation of miR-125b in normal skin.

Overall, our studies implicate miR-125b as a governor of the relative numbers of divisions that a progenitor undergoes prior to committing to a lineage. Given that controlling this property is likely to be of fundamental importance for maintaining the correct size of most organs/tissues, it is intriguing that miR-125a, a related family member, was recently found to be a positive regulator of SC number in the hematopoietic lineage (Guo et al., 2010). Taken together, our findings suggest that the differentiation rheostat role for miR-125b that we've identified here may be a general feature of somatic SCs.

MiR-125b's Target Genes

Our analysis of the global gene expression changes that occur when miR-125b is sustained in HF ORS cells represents the first effort to systematically identify the downstream targets of miR-125b in a postnatal somatic tissue. Our data identified ~800 transcripts that were downregulated within 24 hr of miR-125b induction in both male and female mouse ORS

(E) VDR protein is elevated in lower WT ORS, but reduced in DTG ORS.
(F) RT-PCR of *Vdr* and VDR targets in P79 tail skins (Dox a/P21). GAPDH, reference gene.
(G and H) Accumulative percentile maps for the distribution of VDR targets in P4 ORS microarray results. VDR targets tend to be downregulated after 24 hr Dox induced miR-125b expression in DTG ORS.
(I and J) Relative activities of VDR-responsive element (VDRE) luciferase reporters in (I) DTG MK ± EB1089 ligand (Lig) (10^{-7}M) ± Dox induced miR-125b or (J) WT MK knocked down by anti-miR-125b or scrambled antagomirs (±Lig).
(K) Partial rescue of hair coat defect in DTG mice treated with VDR ligand. DTG and K14-rtTA littermates were treated with Dox a/P48, waxed a/P50 and either injected with PBS or ligand (5 ng/g body weight 3×/wk). Backskins were photographed a/P67.
All error bars represent standard error unless otherwise indicated. All scale bars represent 50 μm unless otherwise indicated.
See also Figures S5 and S6 and Tables S2 and S3.

(Table S2), and importantly, they are highly enriched for predicted conserved miR-125b targets that we also found to be downregulated in WT early bulge versus their progenies. These findings suggest that a considerable portion of these putative miR-125b targets identified in our study are likely to be physiologically relevant.

In the current study, we focused on two miR-125b targets, *Blimp1* and *Vdr.* While their altered expression accounts for many of the miR-125b-induced defects we observed, some perturbations remain unaccounted for by these two miR-125b targets. Notable examples are the remarkable lengthening of HFs and enlargement of lips in DTG mice, which were not observed in either *Blimp1* or *VDR* knockout animals. By contrast, other phenotypes, e.g., the enlarged SGs and blockage of hair growth, were more severe in miR-125b-induced mice than in *Blimp1* or *Vdr* knockout animals. Moreover, because *Blimp1* repression in vivo (Figure 4C) was appreciably greater than that displayed by reporter constructs in vitro (Figure 4E), indirect repression of *Blimp1* transcription might also result from miR-125b induction. When taken together with the fact that excess VDR ligand only partially rescued miR-125b-induced hair loss, it seems likely that additional miR-125b target genes unearthed in our study but as yet untested will be necessary to fully account for the complexities of the DTG phenotype.

In closing, it is notable that like *Blimp1*, *Vdr* has also been reported to be a miR-125 target in a breast carcinoma line (Mohri et al., 2009), raising the possibility that there may be a common core of key miR-125 targets that are coordinately repressed in progenitors and whose activation results in proliferation and commitment. Of the handful of miR-125b targets described to date in other cell types, it is intriguing that *Bmf*, a proapoptotic miR-125b target in human glioma cells, also appeared on our shortlist (Xia et al., 2009, no. 1380), as did the p53 regulator *Trp53inp1*. While *p53* itself is known to be a miR-125b target in several systems (Le et al., 2009; Xia et al., 2009; Zhang et al., 2009; Zhou et al., 2010), this merits further investigation in skin, as it did not surface in our list of putative targets (Table S3). As future studies are conducted, it will be interesting to evaluate the extent to which miR-125's targets will be tailored to suit the general versus specialized needs of SCs in adult tissues.

EXPERIMENTAL PROCEDURES

Mouse Strains and Genetics

Transgenic mice expressing EGFP from a 260 Kb bacterial artificial chromosome (BAC) surrounding the *Sox9* locus were obtained from the GENSAT project (GENSTAT, 2008; Gong et al., 2003). The BAC contained 75 Kb genomic DNA upstream of the *Sox9* coding region, which had been replaced with the EGFP coding sequence. To create *K14-RFP/Sox9-EGFP* double transgenic mice, *Sox9-EGFP* mice were bred to mice regulating *RFP* expression under the control of the *K14* promoter (Vasioukhin et al., 1999). To generate TRE-miR-125b, the mmu-miR-125b coding sequence was amplified by PCR from mouse genomic DNA (Primers 5′-TGCAAAGCTTAGACAGAAAT GAATCTAAATTTTGTG-3′ and 5′-TGCATCTAGACTCAAGGGTGTATTACCAT CACTTC-3′), cloned into HindIII/Xba1 sites of the pTRE2 plasmid (Clontech) and sequenced. Transgenic mice were generated as described (Vasioukhin et al., 1999).

MicroRNA Microarray and Data Analysis

For both miRNA and mRNA microarrays, total RNA samples were extracted from FACS-sorted cells using the miRNeasy Mini Kit (QIAGEN). For mRNA microarray, RNA samples were submitted to the Genomics Core Laboratory of the Memorial Sloan Kettering Cancer Center for cRNA and Amplification and analyzed on Affymetrix mouse 430_2 arrays. For microRNA arrays, samples were submitted to Exiqon. In brief, samples were labeled using the miRCURY Hy3/Hy5 power labeling kit and hybridized on the miRCURY LNA Array (v.11.0) (Exiqon). A sample of Early Bulge, ORS, Matrix, or Basal cells and a reference sample of the corresponding RFP All cells were differentially labeled and cohybridized on the same array. Dye switches were included. The normalized signal ratio between sample and reference was used to represent the relative expression level of each miRNA in each sample. Unsupervised hierarchical clustering analysis was conducted using the cluster software (Eisen et al., 1998). Low expression miRNAs (raw signal intensity $\leq$ 100) were excluded from analyses. miRNA family data were downloaded from the TargetScan website (Lewis et al., 2003, 2005).

SUPPLEMENTAL INFORMATION

Supplemental Information includes six figures and three tables and can be found with this article online at doi:10.1016/j.stem.2011.01.014.

ACKNOWLEDGMENTS

We especially thank (1) Fuchs laboratory members J. Nowak, J. Ross, L. Fish, and S. Williams for developing initial strategies for FACS-purifications and for generating initial P4 HF-SC vs ORS microarray data and T. Chen, Y.-C. Hsu, and H. Zhang for discussions; (2) A. North (RU Bioimaging Resource Center) for assistance with image acquisition; (3) RU Comparative Biology Center, an ALAAC-accredited animal facility, for health care of our mice; and (4) Exiqon for providing LNA-modified antagomirs and other LNA reagents. E.F. is a Howard Hughes Medical Institute Investigator, and L.Z. is an HHMI postdoctoral associate. The work was supported by HHMI and a grant from the NIH.

Received: November 14, 2010
Revised: January 2, 2011
Accepted: January 11, 2011
Published: March 3, 2011

REFERENCES

Alexiou, P., Maragkakis, M., Papadopoulos, G.L., Simmosis, V.A., Zhang, L., and Hatzigeorgiou, A.G. (2010). The DIANA-mirExTra web server: from gene expression data to microRNA function. PLoS ONE *5*, e9171.

Ambros, V. (2004). The functions of animal microRNAs. Nature *431*, 350–355.

Andl, T., Murchison, E.P., Liu, F., Zhang, Y., Yunta-Gonzalez, M., Tobias, J.W., Andl, C.D., Seykora, J.T., Hannon, G.J., and Millar, S.E. (2006). The miRNA-processing enzyme dicer is essential for the morphogenesis and maintenance of hair follicles. Curr. Biol. *16*, 1041–1049.

Baek, D., Villen, J., Shin, C., Camargo, F.D., Gygi, S.P., and Bartel, D.P. (2008). The impact of microRNAs on protein output. Nature *455*, 64–71.

Barrandon, Y., and Green, H. (1987). Three clonal types of keratinocyte with different capacities for multiplication. Proc. Natl. Acad. Sci. USA *84*, 2302–2306.

Bartel, D.P. (2004). MicroRNAs: genomics, biogenesis, mechanism, and function. Cell *116*, 281–297.

Blanpain, C., and Fuchs, E. (2009). Epidermal homeostasis: a balancing act of stem cells in the skin. Nat. Rev. Mol. Cell Biol. *10*, 207–217.

Blanpain, C., Lowry, W.E., Geoghegan, A., Polak, L., and Fuchs, E. (2004). Self-renewal, multipotency, and the existence of two cell populations within an epithelial stem cell niche. Cell *118*, 635–648.

Claudinot, S., Nicolas, M., Oshima, H., Rochat, A., and Barrandon, Y. (2005). Long-term renewal of hair follicles from clonogenic multipotent stem cells. Proc. Natl. Acad. Sci. USA *102*, 14677–14682.

Cotsarelis, G., Sun, T.T., and Lavker, R.M. (1990). Label-retaining cells reside in the bulge area of pilosebaceous unit: implications for follicular stem cells, hair cycle, and skin carcinogenesis. Cell *61*, 1329–1337.

Crist, C.G., and Buckingham, M. (2009). microRNAs gain magnitude in muscle. Cell Cycle *8*, 3627–3628.

Delaloy, C., Liu, L., Lee, J.A., Su, H., Shen, F., Yang, G.Y., Young, W.L., Ivey, K.N., and Gao, F.B. (2010). MicroRNA-9 coordinates proliferation and migration of human embryonic stem cell-derived neural progenitors. Cell Stem Cell *6*, 323–335.

Eisen, M.B., Spellman, P.T., Brown, P.O., and Botstein, D. (1998). Cluster analysis and display of genome-wide expression patterns. Proc. Natl. Acad. Sci. USA *95*, 14863–14868.

Farh, K.K., Grimson, A., Jan, C., Lewis, B.P., Johnston, W.K., Lim, L.P., Burge, C.B., and Bartel, D.P. (2005). The widespread impact of mammalian MicroRNAs on mRNA repression and evolution. Science *310*, 1817–1821.

GENSTAT. (2008). The Gene Expression Nervous System Atlas (GENSAT) Project, NINDS Contracts N01NS02331 and HHSN271200723701C to The Rockefeller University (New York, NY).

Gong, S., Zheng, C., Doughty, M.L., Losos, K., Didkovsky, N., Schambra, U.B., Nowak, N.J., Joyner, A., Leblanc, G., Hatten, M.E., and Heintz, N. (2003). A gene expression atlas of the central nervous system based on bacterial artificial chromosomes. Nature *425*, 917–925.

Greco, V., Chen, T., Rendl, M., Schober, M., Pasolli, H.A., Stokes, N., Dela Cruz-Racelis, J., and Fuchs, E. (2009). A two-step mechanism for stem cell activation during hair regeneration. Cell Stem Cell *4*, 155–169.

Guo, S., Lu, J., Schlanger, R., Zhang, H., Wang, J.Y., Fox, M.C., Purton, L.E., Fleming, H.H., Cobb, B., Merkenschlager, M., et al. (2010). MicroRNA miR-125a controls hematopoietic stem cell number. Proc. Natl. Acad. Sci. USA *107*, 14229–14234.

Gururajan, M., Haga, C.L., Das, S., Leu, C.M., Hodson, D., Josson, S., Turner, M., and Cooper, M.D. (2010). MicroRNA 125b inhibition of B cell differentiation in germinal centers. Int. Immunol. *22*, 583–592.

Hatfield, S.D., Shcherbata, H.R., Fischer, K.A., Nakahara, K., Carthew, R.W., and Ruohola-Baker, H. (2005). Stem cell division is regulated by the microRNA pathway. Nature *435*, 974–978.

Horsley, V., O'Carroll, D., Tooze, R., Ohinata, Y., Saitou, M., Obukhanych, T., Nussenzweig, M., Tarakhovsky, A., and Fuchs, E. (2006). Blimp1 defines a progenitor population that governs cellular input to the sebaceous gland. Cell *126*, 597–609.

Horsley, V., Aliprantis, A.O., Polak, L., Glimcher, L.H., and Fuchs, E. (2008). NFATc1 balances quiescence and proliferation of skin stem cells. Cell *132*, 299–310.

Hsu, Y.-C., Pasolli, H.A., and Fuchs, E. (2011). Dynamics between stem cells, niche, and progeny in the hair follicle. Cell *144*, 92–105.

Ito, M., Yang, Z., Andl, T., Cui, C., Kim, N., Millar, S.E., and Cotsarelis, G. (2007). Wnt-dependent de novo hair follicle regeneration in adult mouse skin after wounding. Nature *447*, 316–320.

Jensen, K.B., Collins, C.A., Nascimento, E., Tan, D.W., Frye, M., Itami, S., and Watt, F.M. (2009). Lrig1 expression defines a distinct multipotent stem cell population in mammalian epidermis. Cell Stem Cell *4*, 427–439.

Lagos-Quintana, M., Rauhut, R., Yalcin, A., Meyer, J., Lendeckel, W., and Tuschl, T. (2002). Identification of tissue-specific microRNAs from mouse. Curr. Biol. *12*, 735–739.

Le, M.T., Teh, C., Shyh-Chang, N., Xie, H., Zhou, B., Korzh, V., Lodish, H.F., and Lim, B. (2009). MicroRNA-125b is a novel negative regulator of p53. Genes Dev. *23*, 862–876.

Lee, R.C., Feinbaum, R.L., and Ambros, V. (1993). The C. elegans heterochronic gene lin-4 encodes small RNAs with antisense complementarity to lin-14. Cell *75*, 843–854.

Lena, A.M., Shalom-Feuerstein, R., Rivetti di Val Cervo, P., Aberdam, D., Knight, R.A., Melino, G., and Candi, E. (2008). miR-203 represses 'stemness' by repressing DeltaNp63. Cell Death Differ. *15*, 1187–1195.

Levy, V., Lindon, C., Harfe, B.D., and Morgan, B.A. (2005). Distinct stem cell populations regenerate the follicle and interfollicular epidermis. Dev. Cell *9*, 855–861.

Lewis, B.P., Shih, I.H., Jones-Rhoades, M.W., Bartel, D.P., and Burge, C.B. (2003). Prediction of mammalian microRNA targets. Cell *115*, 787–798.

Lewis, B.P., Burge, C.B., and Bartel, D.P. (2005). Conserved seed pairing, often flanked by adenosines, indicates that thousands of human genes are microRNA targets. Cell *120*, 15–20.

Li, Q., and Gregory, R.I. (2008). MicroRNA regulation of stem cell fate. Cell Stem Cell *2*, 195–196.

Li, Y.C., Pirro, A.E., Amling, M., Delling, G., Baron, R., Bronson, R., and Demay, M.B. (1997). Targeted ablation of the vitamin D receptor: an animal model of vitamin D-dependent rickets type II with alopecia. Proc. Natl. Acad. Sci. USA *94*, 9831–9835.

Lim, L.P., Lau, N.C., Garrett-Engele, P., Grimson, A., Schelter, J.M., Castle, J., Bartel, D.P., Linsley, P.S., and Johnson, J.M. (2005). Microarray analysis shows that some microRNAs downregulate large numbers of target mRNAs. Nature *433*, 769–773.

Malumbres, R., Sarosiek, K.A., Cubedo, E., Ruiz, J.W., Jiang, X., Gascoyne, R.D., Tibshirani, R., and Lossos, I.S. (2009). Differentiation stage-specific expression of microRNAs in B lymphocytes and diffuse large B-cell lymphomas. Blood *113*, 3754–3764.

Mohri, T., Nakajima, M., Takagi, S., Komagata, S., and Yokoi, T. (2009). MicroRNA regulates human vitamin D receptor. Int. J. Cancer *125*, 1328–1333.

Morris, R.J., Liu, Y., Marles, L., Yang, Z., Trempus, C., Li, S., Lin, J.S., Sawicki, J.A., and Cotsarelis, G. (2004). Capturing and profiling adult hair follicle stem cells. Nat. Biotechnol. *22*, 411–417.

Moss, E.G., Lee, R.C., and Ambros, V. (1997). The cold shock domain protein LIN-28 controls developmental timing in C. elegans and is regulated by the lin-4 RNA. Cell *88*, 637–646.

Nguyen, H., Rendl, M., and Fuchs, E. (2006). Tcf3 governs stem cell features and represses cell fate determination in skin. Cell *127*, 171–183.

Nowak, J.A., Polak, L., Pasolli, H.A., and Fuchs, E. (2008). Hair follicle stem cells are specified and function in early skin morphogenesis. Cell Stem Cell *3*, 33–43.

Oshima, H., Rochat, A., Kedzia, C., Kobayashi, K., and Barrandon, Y. (2001). Morphogenesis and renewal of hair follicles from adult multipotent stem cells. Cell *104*, 233–245.

Palmer, H.G., Martinez, D., Carmeliet, G., and Watt, F.M. (2008). The vitamin D receptor is required for mouse hair cycle progression but not for maintenance of the epidermal stem cell compartment. J. Invest. Dermatol. *128*, 2113–2117.

Rossi, D.J., Jamieson, C.H., and Weissman, I.L. (2008). Stems cells and the pathways to aging and cancer. Cell *132*, 681–696.

Rybak, A., Fuchs, H., Smirnova, L., Brandt, C., Pohl, E.E., Nitsch, R., and Wulczyn, F.G. (2008). A feedback loop comprising lin-28 and let-7 controls pre-let-7 maturation during neural stem-cell commitment. Nat. Cell Biol. *10*, 987–993.

Selbach, M., Schwanhausser, B., Thierfelder, N., Fang, Z., Khanin, R., and Rajewsky, N. (2008). Widespread changes in protein synthesis induced by microRNAs. Nature *455*, 58–63.

Snippert, H.J., Haegebarth, A., Kasper, M., Jaks, V., van Es, J.H., Barker, N., van de Wetering, M., van den Born, M., Begthel, H., Vries, R.G., et al. (2010). Lgr6 marks stem cells in the hair follicle that generate all cell lineages of the skin. Science *327*, 1385–1389.

Stark, A., Brennecke, J., Bushati, N., Russell, R.B., and Cohen, S.M. (2005). Animal MicroRNAs confer robustness to gene expression and have a significant impact on 3′UTR evolution. Cell *123*, 1133–1146.

Taylor, G., Lehrer, M.S., Jensen, P.J., Sun, T.T., and Lavker, R.M. (2000). Involvement of follicular stem cells in forming not only the follicle but also the epidermis. Cell *102*, 451–461.

Tumbar, T., Guasch, G., Greco, V., Blanpain, C., Lowry, W.E., Rendl, M., and Fuchs, E. (2004). Defining the epithelial stem cell niche in skin. Science *303*, 359–363.

Turner, C.A., Jr., Mack, D.H., and Davis, M.M. (1994). Blimp-1, a novel zinc finger-containing protein that can drive the maturation of B lymphocytes into immunoglobulin-secreting cells. Cell *77*, 297–306.

Vasioukhin, V., Degenstein, L., Wise, B., and Fuchs, E. (1999). The magical touch: genome targeting in epidermal stem cells induced by tamoxifen application to mouse skin. Proc. Natl. Acad. Sci. USA *96*, 8551–8556.

Weissman, I.L. (2000). Translating stem and progenitor cell biology to the clinic: barriers and opportunities. Science *287*, 1442–1446.

Wightman, B., Ha, I., and Ruvkun, G. (1993). Posttranscriptional regulation of the heterochronic gene lin-14 by lin-4 mediates temporal pattern formation in C. elegans. Cell *75*, 855–862.

Wu, L., and Belasco, J.G. (2005). Micro-RNA regulation of the mammalian lin-28 gene during neuronal differentiation of embryonal carcinoma cells. Mol. Cell. Biol. *25*, 9198–9208.

Xia, H.F., He, T.Z., Liu, C.M., Cui, Y., Song, P.P., Jin, X.H., and Ma, X. (2009). MiR-125b expression affects the proliferation and apoptosis of human glioma cells by targeting Bmf. Cell. Physiol. Biochem. *23*, 347–358.

Yi, R., and Fuchs, E. (2010). MicroRNA-mediated control in the skin. Cell Death Differ. *17*, 229–235.

Yi, R., O'Carroll, D., Pasolli, H.A., Zhang, Z., Dietrich, F.S., Tarakhovsky, A., and Fuchs, E. (2006). Morphogenesis in skin is governed by discrete sets of differentially expressed microRNAs. Nat. Genet. *38*, 356–362.

Yi, R., Poy, M.N., Stoffel, M., and Fuchs, E. (2008). A skin microRNA promotes differentiation by repressing 'stemness'. Nature *452*, 225–229.

Yi, R., Pasolli, H.A., Landthaler, M., Hafner, M., Ojo, T., Sheridan, R., Sander, C., O'Carroll, D., Stoffel, M., Tuschl, T., and Fuchs, E. (2009). DGCR8-dependent microRNA biogenesis is essential for skin development. Proc. Natl. Acad. Sci. USA *106*, 498–502.

Yu, J., Peng, H., Ruan, Q., Fatima, A., Getsios, S., and Lavker, R.M. (2010). MicroRNA-205 promotes keratinocyte migration via the lipid phosphatase SHIP2. FASEB J. *24*, 3950–3959.

Zhang, Y., Gao, J.S., Tang, X., Tucker, L.D., Quesenberry, P., Rigoutsos, I., and Ramratnam, B. (2009). MicroRNA 125a and its regulation of the p53 tumor suppressor gene. FEBS Lett. *583*, 3725–3730.

Zhao, C., Sun, G., Li, S., Lang, M.F., Yang, S., Li, W., and Shi, Y. (2010). MicroRNA let-7b regulates neural stem cell proliferation and differentiation by targeting nuclear receptor TLX signaling. Proc. Natl. Acad. Sci. USA *107*, 1876–1881.

Zhou, M., Liu, Z., Zhao, Y., Ding, Y., Liu, H., Xi, Y., Xiong, W., Li, G., Lu, J., Fodstad, O., et al. (2010). MicroRNA-125b confers the resistance of breast cancer cells to paclitaxel through suppression of pro-apoptotic Bcl-2 antagonist killer 1 (Bak1) expression. J. Biol. Chem. *285*, 21496–21507.